# Interfacial Reaction between 42Sn-58Bi Solder and Electroless Ni-P/Immersion Au Under Bump Metallurgy during Aging

MOON GI CHO,[1] KYUNG WOOK PAIK,[1] HYUCK MO LEE,[1,3] SEONG WOON BOOH,[2] and TAE-GYU KIM[2]

1.—Department of Materials Science and Engineering, Korea Advanced Institute of Science and Technology, Yusung-Gu, Daejeon 305-701, South Korea. 2.—Computational Science Engineering Center, Samsung Advanced Institute of Technology, Suwon 440-600, South Korea. 3.—E-mail: hmlee@kaist.ac.kr

The interfacial reaction between 42Sn-58Bi solder (in wt.% unless specified otherwise) and electroless Ni-P/immersion Au was investigated before and after thermal aging, with a focus on the formation and growth of an intermetallic compound layer, consumption of under bump metallurgy (UBM), and bump shear strength. The immersion Au layer with thicknesses of 0 μm (bare Ni), 0.1 μm, and 1 μm was plated on a 5-μm-thick layer of electroless Ni-P (with 14–15 at.% P). The 42Sn-58Bi solder balls were then fabricated on three different UBM structures by using screen printing and pre-reflow. A $Ni_3Sn_4$ layer formed at the joint interface after the pre-reflow for all three UBM structures. On aging at 125°C, a quaternary phase, identified as $Sn_{77}Ni_{15}Bi_6Au_2$, was observed above the $Ni_3Sn_4$ layer in the UBM structures that contain Au. The thick $Sn_{77}Ni_{15}Bi_6Au_2$ layer degraded the integrity of the solder joint, and the shear strength of the solder bump was about 40% less than the nonaged joints.

**Key words:** Sn-Bi solder bump, immersion Au under bump metallurgy (UBM), $Sn_{77}Ni_{15}Bi_6Au_2$ phase, consumption of UBM, solid-state aging

## INTRODUCTION

Gold (Au) is widely used in the electronic packaging industry because of its excellent electrical and mechanical properties. For example, Au is used in wire bonding, and the gold alloy 80Au-20Sn has been tested as a solder material for high-temperature applications.[1,2] Moreover, due to its excellent wettability with respect to solder bumps, Au is also used in under bump metallurgy (UBM) systems, such as electroplating Cu/Ni/immersion Au and electroless Ni-P/immersion Au.[3,4]

Intermetallic compounds (IMCs) are generally formed during a reflow of the electronic components that are produced when the UBM reacts with a liquid solder. The IMCs are also formed by the aging of electronic components; that is, when the UBM reacts with a solid solder. An immersion Au layer with a thickness of 0.1 μm completely dissolves in liquid solders of 42Sn-58Bi and 63Sn-37Pb.[5,6] However, the dissolved gold elements are redistributed in the solder and react to form $AuSn_4$ or $(Au,Ni)Sn_4$ during aging.[7–12] The immersion Au is usually plated on a Ni layer of the UBM structure.[13] In this case, $(Au,Ni)Sn_4$ is formed rather than $AuSn_4$, though one report suggests that $(Au,Ni)Sn_4$ is thermodynamically more stable than $AuSn_4$.[8]

We therefore investigated the interfacial reaction of the 42Sn-58Bi solder and the electroless Ni-P/immersion Au UBM. The 42Sn-58Bi solder alloy is a Pb-free solder material with a low melting point. We bumped the 42Sn-58Bi solder alloy on three different types of UBM: bare Ni-P UBM, electroless Ni-P/immersion Au (0.1 μm) UBM, and electroless Ni-P/immersion Au (1 μm) UBM. We then conducted thermal aging at 125°C for up to 1000 h. Next, we investigated the phase type of IMC in each joint and explored the growth of the interfacial IMC layer during aging. Additionally, we studied how the IMCs affect the shear strength of the joint after thermal aging.

(Received March 20, 2005; accepted August 10, 2005)

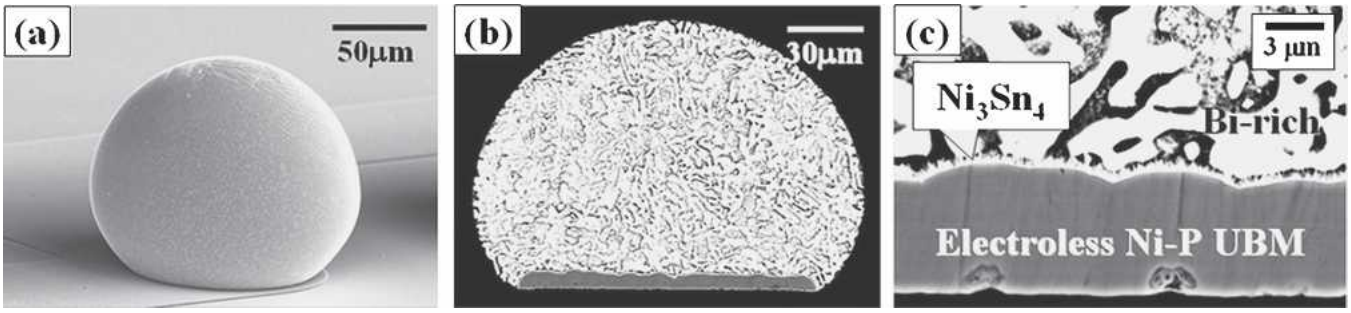


Fig. 1. (a) Screen-printed 42Sn-58Bi solder bump on electroless Ni-P UBM; (b) cross-sectioned SEM image of the 42Sn-58Bi solder bump; and (c) interface of 42Sn-58Bi solder and electroless Ni-P UBM after the pre-reflow.

## EXPERIMENTAL PROCEDURES

After using lithography to pattern circular Al pads (with a diameter of 100 μm and a thickness of 1 μm) on Si wafers, we fabricated three types of UBM on the zincate-treated Al pads: bare electroless Ni-P (5 μm), electroless Ni-P (5 μm)/immersion Au (0.1 μm), and electroless Ni-P (5 μm)/immersion Au (1 μm). The P content of the electroless Ni-P UBM was about 14–15 at.%. We then screen printed the 42Sn-58Bi solder on each UBM. Next, we performed the flux activation for 1 min at 110°C and a pre-reflow with a dwell time of 1 min and a peak temperature of 170°C. A pre-reflow means a necessary step to create the solder bump after the solder paste has been printed. After the pre-reflow, we fabricated the solder bumps, as shown in Fig. 1. The thermal aging of each sample was performed at 125°C for 125 h, 250 h, 500 h, and 1000 h. We then sectioned all the samples and etched them with methanol-nitric hydrochloric acid. Finally, we examined the microstructures with scanning electron microscopy (SEM), and we examined the compositions with the following: energy-dispersive x-ray spectroscopy (EDS), wavelength-dispersive x-ray spectrometry (WDS) in electron probe microanalysis, and x-ray diffractometry (XRD) using Cu $K\alpha_1$.

## RESULTS AND DISCUSSION

Figure 2 shows cross-sectional SEM images of solder bumps aged at 125°C. The lamellar structure of the Sn-Bi solder, which coarsened with prolonged

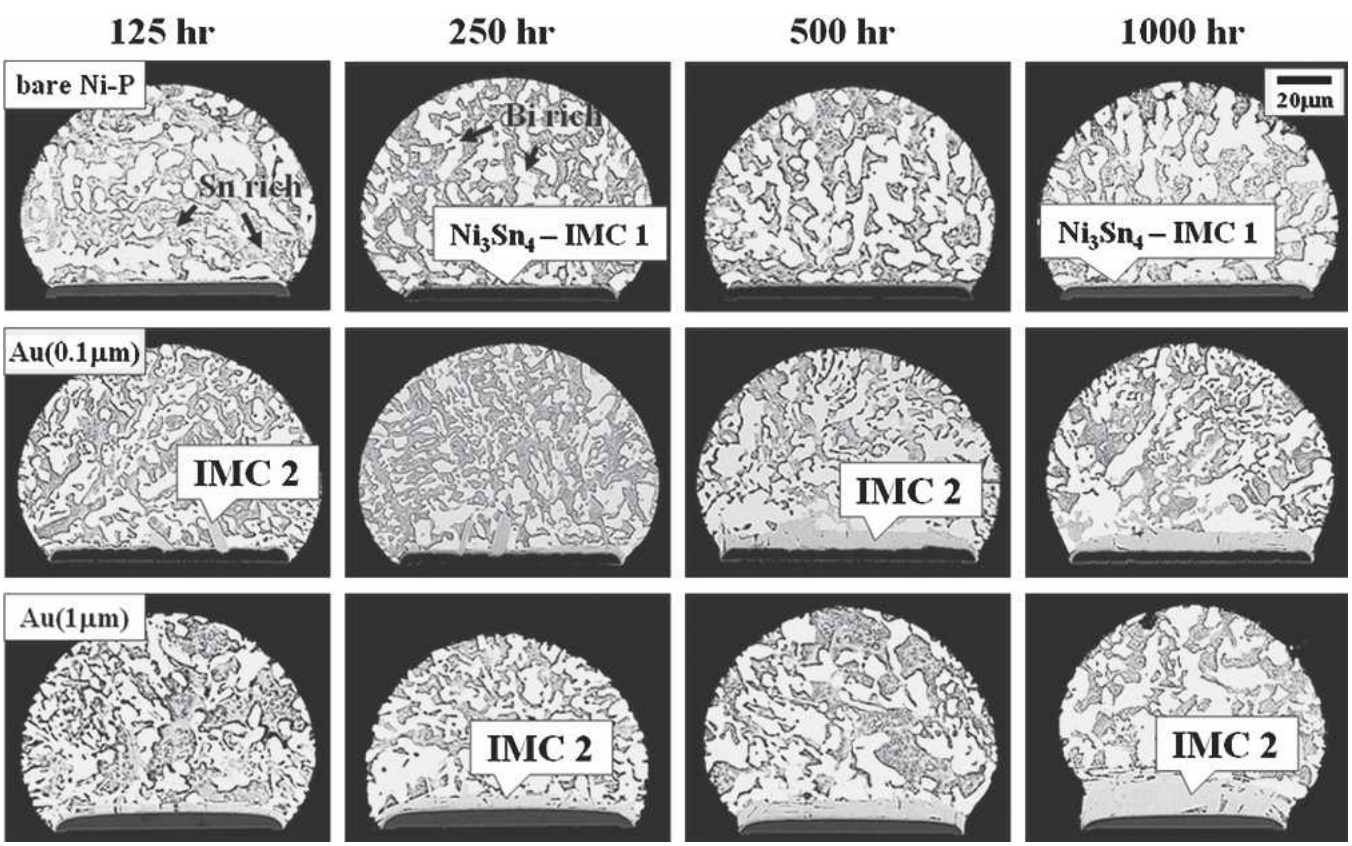


Fig. 2. Cross-sectioned SEM images of solder bump joints with three different UBM structures after solid-state aging at 125°C for 1000 h. IMC1 is identified as $Ni_3Sn_4$, and IMC2 is identified as $Sn_{77}Ni_{15}Bi_6Au_2$. The UBM structure in the first row is bare electroless Ni-P, while the UBM structures in the second and third rows are electroless Ni-P (5 μm)/immersion Au (0.1 μm) and electroless Ni-P (5 μm)/immersion Au (1 μm), respectively.

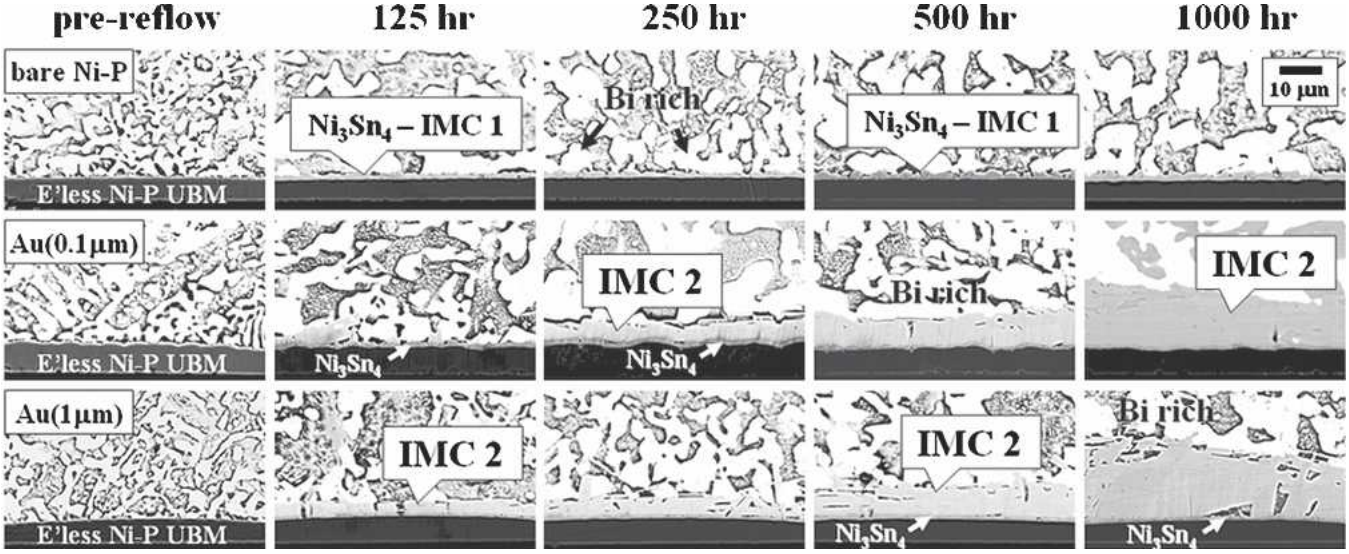


Fig. 3. Enlarged interfaces of 42Sn-58Bi solder joints with three different UBM structures after solid-state aging at 125°C for 1000 h. IMC1 is identified as $Ni_3Sn_4$, and IMC2 is identified as $Sn_{77}Ni_{15}Bi_6Au_2$. The UBM structure in the first row is bare electroless Ni-P, while the UBM structures in the second and third rows are electroless Ni-P (5 μm)/immersion Au (0.1 μm) and electroless Ni-P (5 μm)/immersion Au (1 μm), respectively.

aging, is composed of a Sn-rich region (dark contrast) and a Bi-rich region (bright contrast) in each UBM structure. Although we observed no intermetallic phase inside the solder bump, we did observe an IMC layer at the joint interface. Figure 3 shows enlarged images of the joint interface.

Generally, $Ni_3Sn_4$ IMCs form at the interface of Sn-Bi or Sn-Pb solders on electroless Ni-P/immersion Au after a reflow.[5,6] The interfacial IMC phase of bare Ni is $Ni_3Sn_4$, which comprises about 57–58 at.% Sn and about 42–43 at.% Ni. We named this phase IMC1. The same type of $Ni_3Sn_4$ was observed at the interface of Sn-Bi and the UBM structures that contain immersion Au layers (with a thickness of 0.1 μm and 1 μm). Figure 3 shows another IMC phase (named IMC2) in both the UBM structures that contain immersion Au; the composition of this phase differs from that of $Ni_3Sn_4$. As measured by EDS, this phase comprised Sn (79–80 at.%), Ni (12–13 at.%), Bi (5–6 at.%), and Au (1–2 at.%).

To determine the composition of IMC2 more exactly, we performed WDS mapping of electron-probe microanalysis. Figure 4 shows the WDS mapping images of the joint interface on the electroless Ni-P (5 μm)/immersion Au (0.1 μm) aged for 1000 h. In results that are similar to the EDS results, it comprised four elements: Sn (77.5 at.%), Ni (15 at.%), Bi (5.6 at.%), and Au (1.9 at.%). We then identified the IMC2 phase as the quaternary $Sn_{77}Ni_{15}Bi_6Au_2$.

Next, we performed an XRD test for the IMC2 area, which we identified as $Sn_{77}Ni_{15}Bi_6Au_2$. In addition, Fig. 5a, which shows the XRD patterns of IMC2, shows the XRD patterns of Sn, Bi, and $Ni_3Sn_4$ together.[14–16] There were six additional peaks, as marked by arrows, which do not correspond to any of them. Notably, the six additional peaks do not match the patterns of the IMC phases that contain Au, as exemplified by $AuSn_2$ in Fig. 5b, $AuSn_4$ in Fig. 5c, and $(Au,Ni)Sn_4$ in Fig. 5d.[17–19] The new peaks seem to have come from $Sn_{77}Ni_{15}Bi_6Au_2$.

The IMC2, $Sn_{77}Ni_{15}Bi_6Au_2$, is similar to $(Au,Ni)Sn_4$ formed at the interface in the 63Sn-37Pb solder with respect to the elements and the formation site.[7–9] The atomic ratio of Sn to the other elements is about 4:1, and its formation occurred between the solder bump and the UBM, especially above the $Ni_3Sn_4$ layer. However, the XRD results clearly show that $Sn_{77}Ni_{15}Bi_6Au_2$ has a different crystalline structure than $(Au,Ni)Sn_4$, though the exact crystalline structure has not yet been revealed. It is therefore difficult to assert that $Sn_{77}Ni_{15}Bi_6Au_2$ is based on $(Au,Ni)Sn_4$. Further powder-type XRD analysis is needed.

We observed both the IMC1 and IMC2 phases on UBM structures that contain Au, whereas we observed only the IMC1 phase in the bare Ni UBM. Only 2 at.% Au was involved in the formation of IMC2, $Sn_{77}Ni_{15}Bi_6Au_2$. Young et al. studied the joint interfacial reaction of the eutectic Sn-Bi solder with electroless Ni-based multimetallization (Ni-5.5 wt.% P and Ni-12 wt.% P) and found the ternary IMC comprised Sn (78–80 at.%), Ni (12 at.% to 16 at.%), and Bi (5 at.% to 8 at.%) on aging at 110°C.[20] The compositions were measured by electron-probe microanalysis. Aging at 130°C accelerated the growth of the ternary IMC and resulted in the formation of additional $Ni_3Sn_4$. An average amount of 0.68 at.% Au was observed in the ternary IMC region, but it was regarded as the dissolved Au in the solder bulk according to Young et al.'s interpretation. It is not clear why a lesser amount of Au was detected in their study compared with this work. However, Fig. 4e shows that the elemental distribution of Au is very homogeneous. Additional consideration on the detection capability of the thick qua-

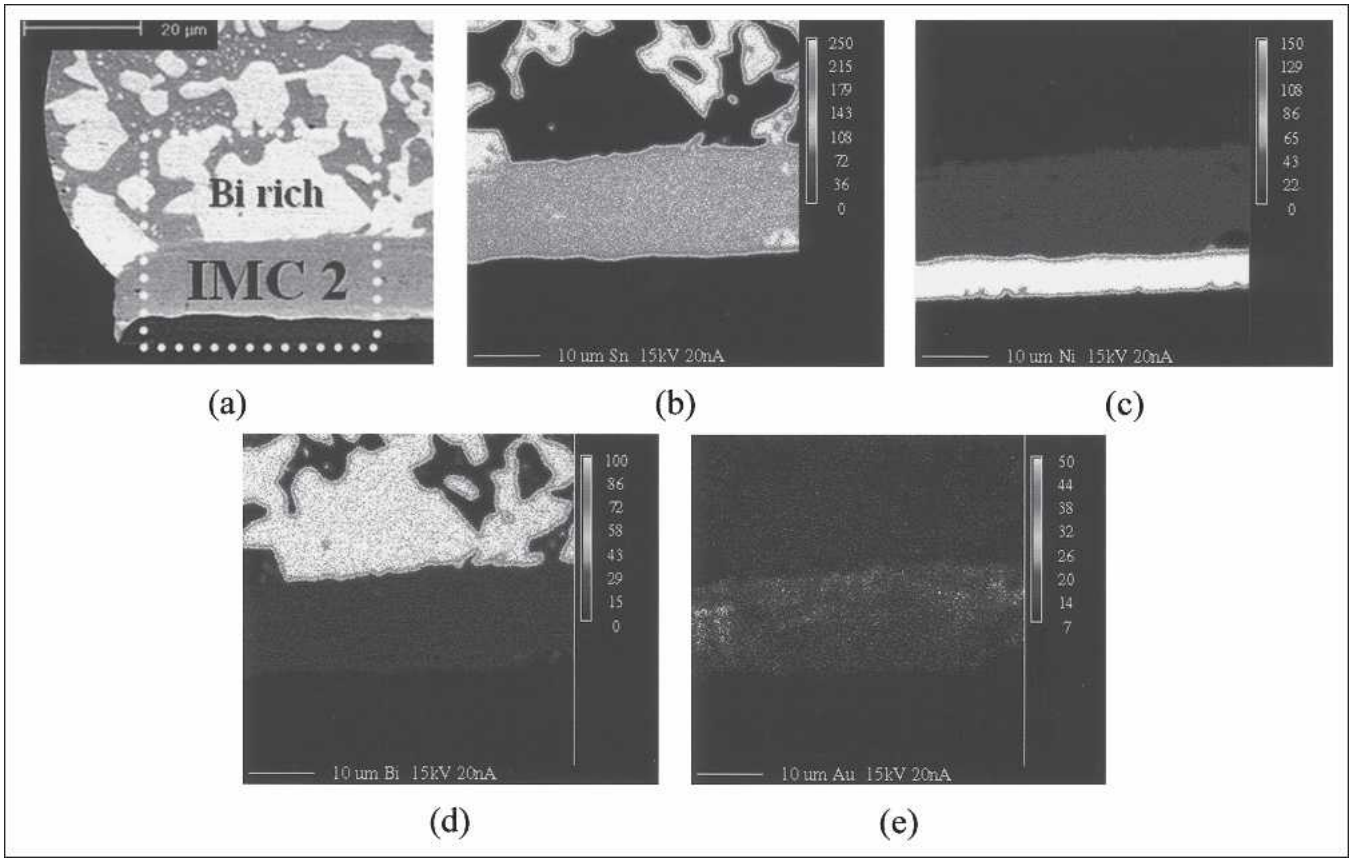


Fig. 4. WDS mapping images of the IMC2 phase at the joint interface after aging at 125°C for 1000 h. The UBM was electroless Ni-P (5 μm)/immersion Au (0.1 μm): (a) SEM micrograph of IMC2, (b) Sn mapping, (c) Ni mapping, (d) Bi mapping, and (e) Au mapping.

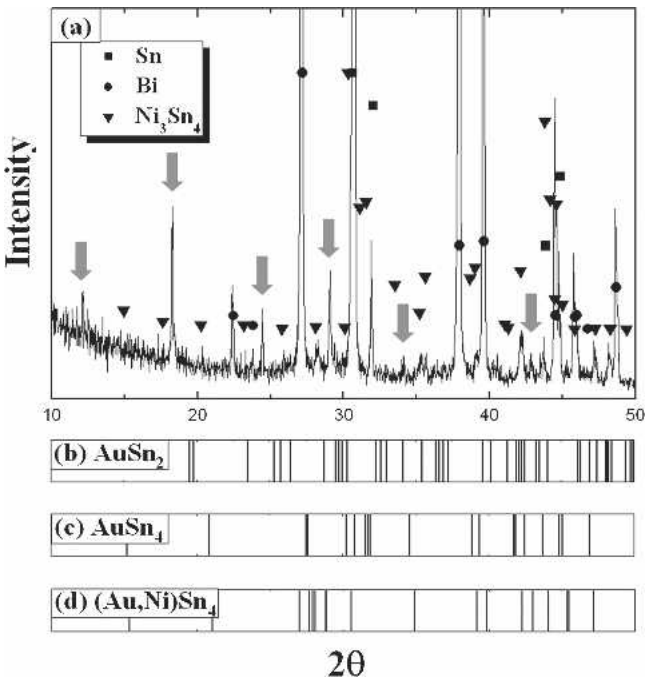


Fig. 5. (a) XRD patterns of the IMC2 region; (b) calculated XRD patterns of $AuSn_2$ from Ref. 17; (c) calculated XRD patterns of $AuSn_4$ from Ref. 18; and (d) calculated XRD patterns of $(Au,Ni)Sn_4$ from Ref. 19.

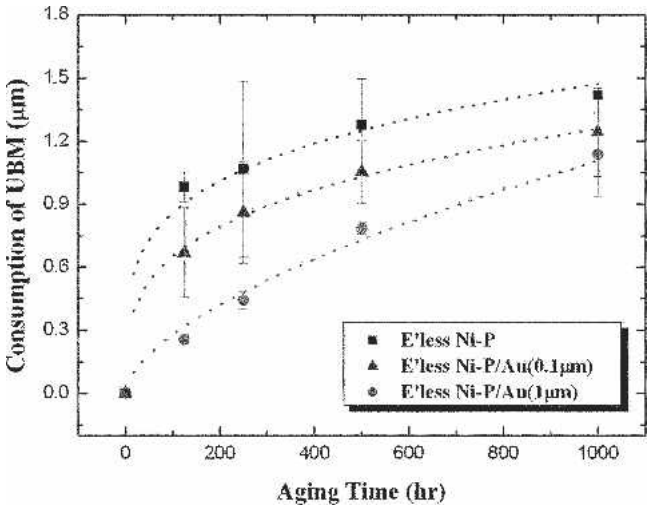


Fig. 6. Consumption of UBM during solid-state aging compared with the pre-reflow conditions.

ternary IMC2 layer also strongly supports the finding that IMC2 is quaternary containing 2 at.% Au.

Kang and Kim studied the microstructure of ultrasmall (about 50 μm) eutectic Sn-Bi bumps on Au/Ni/Ti UBM as a function of cooling rate in soldering.[21] They observed the faceted and polygonal IMC in slowly solidified solder bumps and joints. They confirmed the IMC as $(Au,Bi,Ni)Sn_2$ by an XRD test only. The IMC particles were found in the solder matrix as well as at the joint interface. Contrary to their observation, we did not detect the $(Au,Bi,Ni)Sn_2$ phase in the current study and the XRD pat-

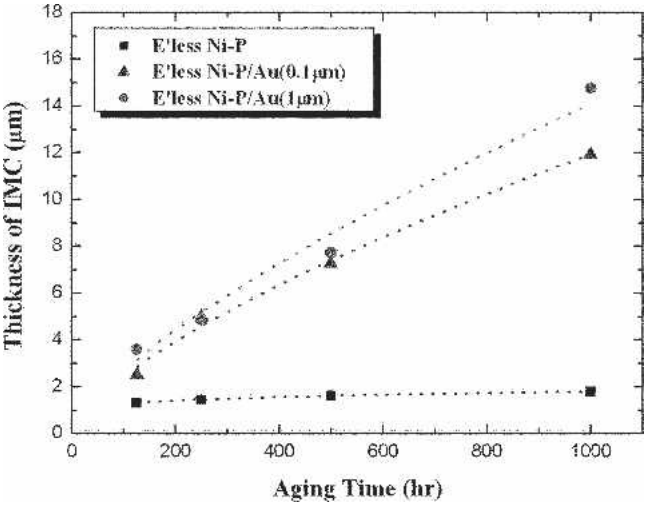


Fig. 7. Growth of the IMC layer (both IMC1 and IMC2) during solid-state aging compared with the pre-reflow conditions.

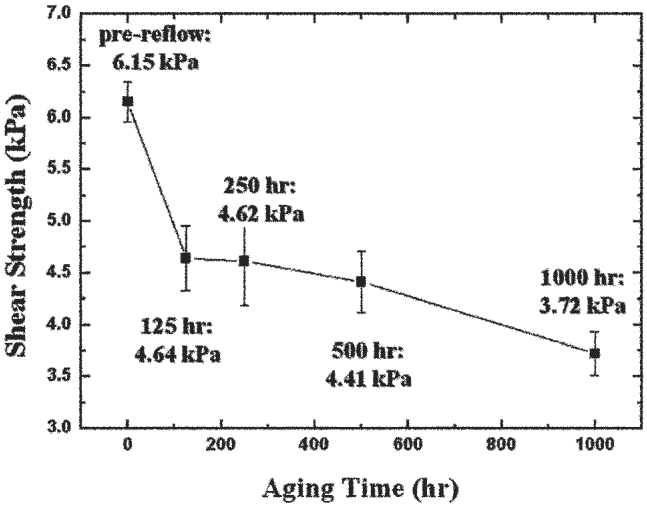


Fig. 8. Variation of shear strength of the 42Sn-58Bi solder bump on electroless Ni-P/immersion Au (0.1 μm) with aging.

terns in Fig. 5a and b do not identify IMC2 as $AuSn_2$ based. It is highly likely that the difference comes from the rather slow cooling rates and the electroplated Ni layer in Kang and Kim's study.

Figure 6 compares a plot of the UBM consumed during the solid-state aging with the pre-reflow conditions. As stated earlier, the pre-reflow condition means the as-formed solder bump state. As expected, the UBM consumption increased with aging. The degree of consumption was highest for the bare Ni, followed by the electroless Ni-P (5 μm)/immersion Au (0.1 μm) and then the electroless Ni-P (5 μm)/immersion Au (1 μm). Figure 7 shows how the IMC layer (both IMC1 and IMC2) grew during aging on the basis of the pre-reflow. The growth of the IMC layer is lowest for the bare Ni, followed by the electroless Ni-P (5 μm)/immersion Au (0.1 μm) and then the electroless Ni-P (5 μm)/immersion Au (1 μm).

The solder joint with the bare Ni UBM simultaneously shows the highest UBM consumption and the lowest IMC growth. At first glance, this result seems contradictory. However, the result originates from the fact that although the IMC layer comprises only $Ni_3Sn_4$ (IMC1) in the bare Ni, the layer comprises IMC2 as well as IMC1 in the UBM structure that contains Au. The buildup of the IMC2 layer that contains Au, $Sn_{77}Ni_{15}Bi_6Au_2$, is predominant in the UBM structures that contain Au. The IMC2 layer thickens quickly and consumes the nearby Sn elements. As shown in Fig. 7, the IMC2 layer is much thicker than the $Ni_3Sn_4$ layer (IMC1). Therefore, the growth of the entire IMC layer is greater in UBM structures that contain Au than in bare Ni. In terms of consuming the UBM, fewer Ni atoms are needed in the atom ratio when forming IMC2, $Sn_{77}Ni_{15}Bi_6Au_2$, than when forming IMC1, $Ni_3Sn_4$. Therefore, less UBM is consumed in UBM structures that contain Au than in bare Ni UBM.

For the bump shear test, we used a typical solder bump joint with electroless Ni-P (5 μm)/immersion Au (0.1 μm) aged for 1000 h. As shown in Fig. 8, the shear strength was 3.72 kPa after 1000 h aging but 6.15 kPa immediately after the pre-reflow. The shear strength decreased greatly, by about 40%, and the main drop had already occurred after 125 h of aging. To find out the cause of the large drop in shear strength, we plotted the shear strength with the shear distance during the bump shear test shown in Fig. 9. The x-axis represents the distance the stylus moved through the solder bump, and the y-axis represents the shear strength at any given moment. While enduring the movement of the stylus, the solder bump in the pre-reflow state was deformed and fractured, implying a ductile fracture mode. However, after being aged for 1000 h, the solder bump fractured suddenly without enduring the movement of the stylus, implying a brittle fracture mode.

For confirmation, we investigated the fracture surface. As shown in Fig. 10, the fracture site inside

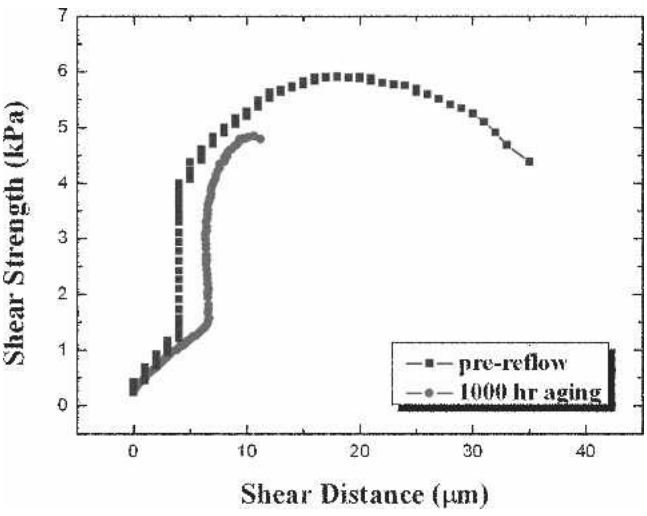


Fig. 9. Plot of shear strength and shear distance measured as the stylus moved through the solder bump under the two conditions of a pre-reflow and 1000 h of aging.

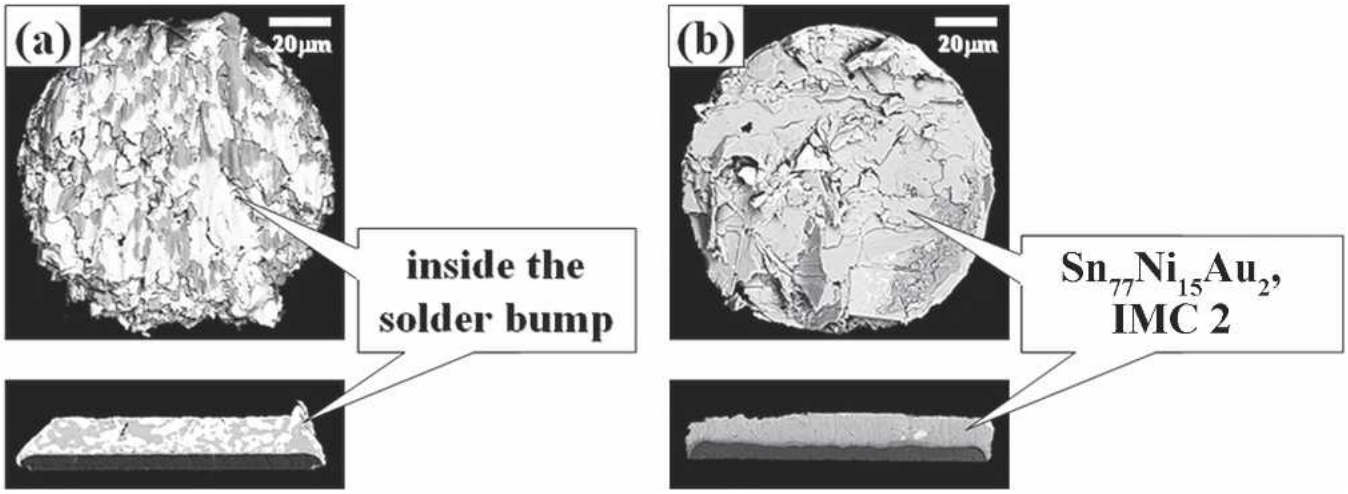


Fig. 10. Top-view and cross-sectional images of the fracture surface after the bump shear test: (a) the pre-reflow and (b) 1000 h of aging.

the solder bump had a fracture surface that was rough in the pre-reflow condition; in contrast, the fracture site at the interface of the IMC layer had a fracture surface that was clean after 1000 h of aging. After extended aging, as revealed in the fracture surface, the large decrease in shear strength seems to have resulted from the formation of the thick $Sn_{77}Ni_{15}Bi_6Au_2$ IMC2 layer. The thick interfacial IMC phase must have been brittle, and it decreased the strength of the adhesion between the solder bump and the interfacial IMC.[22] Therefore, when we performed the shear test for the solder bump joint with electroless Ni-P (5 μm)/immersion Au (0.1 μm) after aging, the fracture occurred along the interface of the IMC layer and the shear strength decreased greatly.

## SUMMARY

We investigated the interfacial reaction between 42Sn-58Bi solder and electroless Ni-P/immersion Au after thermal aging. The interfacial IMC phase for bare Ni was $Ni_3Sn_4$. We also observed the same type of $Ni_3Sn_4$ at the interface between Sn-Bi and UBM structures containing immersion Au layers (0.1-μm and 1-μm thick). Moreover, we identified another IMC phase (named IMC2) as quaternary $Sn_{77}Ni_{15}Bi_6Au_2$.

The degree of consumption was highest for the bare Ni, followed by electroless Ni-P/immersion Au (0.1 μm) and then electroless Ni-P/immersion Au (1 μm). The growth of the IMC layer (both IMC1 and IMC2) during aging was lowest for the bare Ni, followed by the electroless Ni-P/immersion Au (0.1 μm) and then the electroless Ni-P/immersion Au (1 μm). The IMC2 layer that contained Au, $Sn_{77}Ni_{15}Bi_6Au_2$, was much thicker than the $Ni_3Sn_4$ layer (IMC1). Therefore, the growth of the entire IMC layer is greater in UBM structures that contain Au than in those with bare Ni.

For the bump shear test, we used a typical solder bump joint with electroless Ni-P/immersion Au (0.1 μm) aged for 1000 h. The formation of the thick $Sn_{77}Ni_{15}Bi_6Au_2$ IMC2 layer after aging caused a fracture along the interface of the IMC layer, and the shear strength decreased enormously.

## ACKNOWLEDGEMENTS

This study was supported by the Center for Electronic Packaging Materials (CEPM), Korea Science and Engineering Foundation (KOSEF).

## REFERENCES

1. J.H. Kim, S.W. Jeong, and H.M. Lee, *Mater. Trans.* 43, 1873 (2002).
2. S.S. Kim, J.H. Kim, S.W. Booh, T.G. Kim, and H.M. Lee, *Mater. Trans.* 46, 2400 (2005).
3. T.A. Powers, T.J. Singer, and J.A. Clum, *J. Electron. Mater.* 23, 773 (1994).
4. R.B. Cinque and J.W. Morris, Jr., *J. Electron. Mater.* 23, 533 (1994).
5. C.-S. Huang, J.-H. Yeh, B.-L. Young, and J.-G. Duh, *J. Electron. Mater.* 31, 1230 (2002).
6. C.Y. Lee and K.L. Lin, *Jpn. J. Appl. Phys.* 33, 4708 (1994).
7. K. Zeng and K.N. Tu, *Mater. Sci. Eng., R* 38, 55 (2002).
8. K.Y. Lee, M. Li, and K.N. Tu, *J. Mater. Res.* 18, 2562 (2003).
9. C.E. Ho, W.T. Chen, and C.R. Kao, *J. Electron. Mater.* 30, 379 (2001).
10. K.Y. Lee and M. Li, *J. Electron. Mater.* 32, 906 (2003).
11. C.M. Liu, C.E. Ho, W.T. Chen, and C.R. Kao, *J. Electron. Mater.* 30, 1152 (2001).
12. K.Y. Lee and M. Li, Metall. *Mater. Trans.* 32A, 2666 (2001).
13. B.-L. Young and J.-G. Duh, *J. Electron. Mater.* 30, 878 (2001).
14. V.T. Deshpande and D.B. Sirdeshmukh, *Acta Crystallogr.* 15, 294 (1962).
15. P. Cucka and C.S. Barrett, *Acta Crystallogr.* 15, 865 (1962).
16. H. Nowotny and K. Schubert, *Z. Metallkd.* 37, 23 (1946).
17. K. Schubert, *Z. Metallkd.* 50, 146 (1959).
18. K. Schubert and U. Rosler, *Z. Metallkd.* 41, 298 (1950).
19. L. Zavalij, A. Zribi, R.R. Chromik, S. Pitely, P.Y. Zavalij, and E.J. Cotts, *J. Alloys Compounds* 334, 79 (2002).
20. B.-L. Young, J.-G. Duh, and G.-Y. Jang, *J. Electron. Mater.* 32, 1463 (2003).
21. U.-B. Kang and Y.-H. Kim, *J. Electron. Mater.* 33, 61 (2004).
22. D.R. Frear, F.M. Hosking, and P.T. Vianco, *Proc. Materials Developments in Microelectronic Packaging Conf.* (Materials Park, OH: ASM International, 1991), pp. 229–240.